Crystallization of Monotropic Liquid Crystalline Polycarbonates Based on a Methyl-Stilbene Mesogen and a Methylene-Containing Flexible Spacer

Yao-Yi Cheng and Peggy Cebe*

Department of Materials Science and Engineering, Massachussetts Institute of Technology, Cambridge, Massachusetts 02139

Heidi Schreuder-Gibson, Aaron Bluhm, and Walter Yeomans

U.S. Army Natick Research, Development and Engineering Center, Natick, Massachusetts 01760

Received March 7, 1994; Revised Manuscript Received May 24, 1994®

ABSTRACT: Crystallization behavior has been studied for a series of recently synthesized liquid crystalline polycarbonates[1] based on a methyl-substituted stilbene mesogen and a methylene-containing flexible spacer. The stability of the nematic phase and its relationship to three-dimensional crystallinity were studied. Development of crystallinity was followed by isothermal and nonisothermal crystallization using differential scanning calorimetry (DSC) and polarizing optical microscopy. A monotropic liquid crystal phase is identified for these polycarbonates. The multiple melting endotherms seen in the heating scan are assigned to the melting of crystals forming either from the mesophase (melting at higher temperature) or from the isotropic phase (melting at lower temperature). The number, n, of $-(CH_2)-$ units in the flexible spacer affects the transition temperatures seen in the cooling and heating scans. Only a weak odd–even effect is seen in the upper melting of the heating scan from $n = 5$ to 8. In this range of spacer length, the region of stability of the liquid crystal phase seen in the cooling scan becomes smaller. When the length of the spacer becomes greater than that of the mesogen ($n \geq 9$), all the transition temperatures drop.

1. Introduction

One major class of liquid crystalline polymers (LCP) is the main chain liquid crystalline polymer, which is a linear molecule consisting of a rigid mesogen alternating with a flexible spacer. From a thermodynamic point of view, the liquid crystalline phase can be identified to be either enantiotropic or monotropic.[2] The *enantiotropic* mesophase is thermodynamically stabilized with respect to both the isotropic phase and the crystalline phase, within the temperature range from the melting point, T_m, to the temperature of isotropization, T_i. It is observed as reversible in both heating and cooling. On the other hand, the *monotropic* mesophase cannot be observed in heating and can be observed in cooling only provided that the crystallization process is suppressed due to supercooling. It has been found that the monotropic mesophase exists in several kinds of main chain thermotropic liquid crystalline polymers, such as poly(ester imides),[3] polyurethanes,[4,5] and polyethers and copolyethers.[6-10] It has also been found that some enantiotropic LCPs can behave like monotropic LCPs after an annealing process.[11]

The behavior of these monotropic LCPs is strongly related to the shape of the monomer unit and the conformation of the polymer chain. One interesting characteristic is the existence of a kink in the polymer chain, which plays an important role in the interaction between the polymer chains. A kink can permanently exist in a polymer chain, as, for example, in polyurethane LCPs.[4,5] This particular kink is caused by two urethane linkages in the meta positions with respect to the benzene ring. Due to the interchain hydrogen bonding forming within the urethane linkage by adjacent polymer chains, these LCPs form an ordered monotropic mesophase. The order is preserved in the crystalline phase which forms from the mesophase. A kink can also exist in a polymer chain as one of the conformational isomers. Percec's liquid crystalline polyethers and copolyethers[6-10] are examples. Instead of being linked by a rigid group, two benzene rings are connected by two methylene linkages to form a flexible rodlike mesogen. The formation of the monotropic mesophase depends on the degree of alignment of polymer chains caused by their cooperative movement.

It is well-known that for main chain LCPs, both the mesogen and the flexible spacer contribute to the orientational order that characterizes the transition from the isotropic (i) phase to the liquid crystal (lc) mesophase. From the intercept and the slope of ΔH_{i-lc} and ΔS_{i-lc} versus the number of methylene units in the flexible spacer, Blumstein first obtained the contribution from the mesogen and the flexible spacer, respectively.[12] The former was assigned as the orientation contribution and the latter as the conformation contribution. Blumstein's polyesters showed an odd–even effect in ΔH_{i-lc} and ΔS_{i-lc} versus n, the number of methylene units in the flexible spacers.[12,13] The value is higher when n is even. This effect can be understood by considering that the degree of alignment of the polymer chains within the mesophase is higher for the even series than for the odd series, when the methylene units in the flexible spacer have all-trans conformation.[14,15] This effect is usually observed and can be theoretically justified[16,17] for those polymers with rigid rod mesogens. However, for Percec's polyethers with flexible mesogens,[10] ΔH_{i-lc} and ΔS_{i-lc} increase linearly with the number of methylene units in the flexible spacers. This phenomenon was explained by the coupled action of the flexible mesogen and the flexible spacer.

In this work, we report on characterization and crystallization studies of α-methyl-stilbene polycarbonates (HMS-n) whose synthesis has been reported previously.[1] The chemical repeat unit for these polymers is

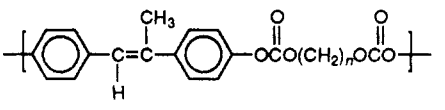

The flexible spacer number, n, equals 4–10 and 12. A

* To whom correspondence should be addressed.
® Abstract published in *Advance ACS Abstracts*, August 1, 1994.

0024-9297/94/2227-5440$04.50/0

monotropic mesophase was identified for these HMS polycarbonates. Like some other monotropic LCPs mentioned above, HMS polycarbonates also have kinks in their polymer chains caused by the conformational isomers of the carbonate linkage. If the two bonds adjacent to the carbonate linkage have a trans conformation, then HMS polycarbonates will have a linear shape.

Stilbene-containing polymers have been widely studied due to the straightforward synthesis of the stilbene, which was evaluated 56 years ago as a synthetic hormone.[18] α-Methylstilbene polyethers[19] and α-methylstilbene polyesters[14,20] were both enantiotropic liquid crystalline polymers. The polyethers displayed a lower melting temperature than the polyesters. All of these α-methylstilbene polymers showed an odd–even effect in both the melting temperature, T_m ($T_m = T_{k-lc}$), and the transition temperature from the liquid crystalline phase to the isotropic phase, T_i ($T_i = T_{lc-i}$), vs n. When n is even, both transition temperatures tend to be higher.

In this work, we report on the crystallization and melting behavior of α-methylstilbene polycarbonates.[1] In contrast to the enantiotropic stilbene-based polyethers and polyesters, HMS polycarbonates are monotropic LCPs. Also, there is no odd–even effect seen in any of the transition temperatures vs the flexible spacer number. Finally, there are different trends in the phase transition temperatures for $n \leq 8$ compared with those of higher n value. These differences in thermal behavior can be related directly to differences in the chemical structure of the linking groups and to the relative lengths of the flexible spacer and mesogen.

2. Experimental Section

2.1. Materials. The synthesis of HMS polycarbonates followed the method of Sato[21] and was published separately.[1] The resultant LCPs were soluble in chloroform and obtained as fine white powders, except for $n = 7$ and 9, which were obtained as white, very fibrous products. All polymers studied in this research have reasonably high molecular weights, in the range 11000–54800 with distributions (M_w/M_n) close to 2 as reported previously.[1]

2.2. Differential Scanning Calorimetry (DSC). Thermal properties of materials were studied using a Perkin-Elmer DSC-4 or DSC-7. Indium was used to calibrate the temperature and the heat of fusion. All materials studied had a sample weight range of 2.5–6.5 mg. The studies that were done included heating and cooling at fixed rates, the effect of crystallization temperature on crystallization time and melting temperature, and the effect of crystallization time on melting temperature.

The first approach involved heating and cooling at fixed rates over a wide temperature interval. The sample was heated to 200 °C and held at that temperature for 2.5–3 min, then cooled at a rate of 10 °C/min to 50 °C, and then heated at 10 °C/min to 200 °C. This study was done for all HMS-n samples. In addition, HMS-6–9 were cooled and heated at 5, 20, and 50 °C/min. This study was designed to test the dependence of the mesophase to isotropic transition on cooling rate.

The next study was isothermal crystallization for HMS-5–9. The sample was melted at 190 °C for about 3 min and then quenched at −50 °C/min to a crystallization temperature T_c and held isothermally until the crystallization was finished. The T_cs were specifically chosen for each HMS sample in advance. Because all HMS-5–8 materials have close crystallization temperatures, we chose the same crystallization temperatures in the range between 138 and 144 °C for these samples. Exothermic heat flow as a function of time was measured. Here we were interested in the effect of the flexible spacer number on the isothermal crystallization kinetics.

The next study involved immediate rescan after isothermal crystallization for HMS-5, -6, -8, and -9. After staying at T_c isothermally until crystallization was finished, the sample was immediately heated at 5 °C/min to 190 °C without cooling. This immediate rescan technique avoids the formation of imperfect crystals during cooling to room temperature and thus results in a cleaner endothermic response.

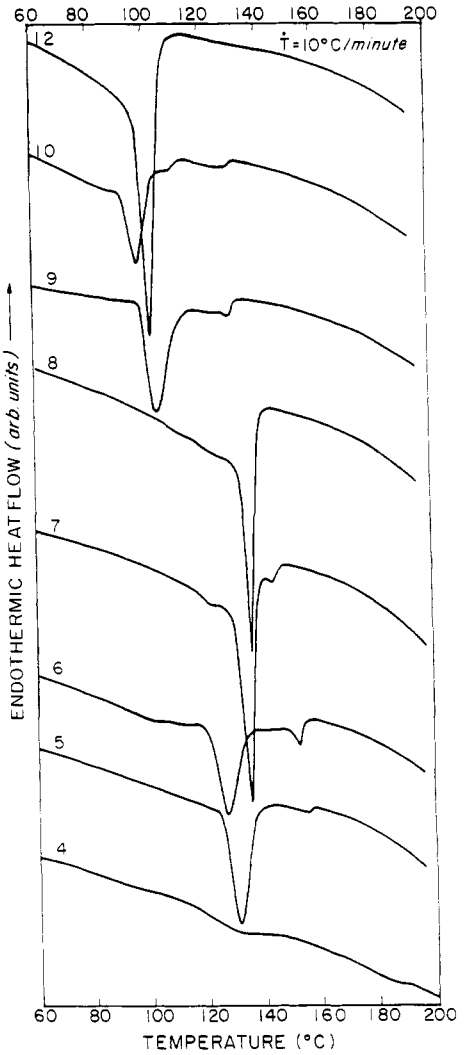

Figure 1. DSC thermograms of HMS-4–10 and -12 at 10 °C/min cooling rate.

HMS-5 and HMS-9 were studied by a variety of other thermal approaches. HMS-9 was held at T_c = 114 °C and HMS-5 at T_c = 140 °C until crystallization was finished and then immediately heated at 1, 2, or 5 °C/min. Finally, the effect of crystallization time was studied for HMS-9 at T_c = 114 °C and for HMS-5 at T_c = 147 °C. Samples were held isothermally at the crystallization temperature for different times and then immediately heated at 5 °C/min to 190 °C, without cooling to room temperature.

2.3. Optical Microscopy. A Zeiss microscope was equipped with a turret containing long working distance objective lenses for use with the Mettler hot stage. The long working distance protects the lens from aberrations that might result from exposure to elevated temperatures. For HMS-n, samples of powder were placed on glass slides and covered with a glass cover slip. These were inserted into the hot stage at room temperature and the stage controller was set to heat and then cool the samples at a fixed rate. Samples were studied using polarized transmitted light geometry, and the analyzer was placed at 90° to the polarizer. The change in transmittance was recorded simultaneously as the sample heated.

Crystallization studies were done on HMS-5. The polymer was heated to 190 °C, held at that temperature for 2.5 min, and then cooled at 20 °C/min for isothermal crystallization to 127 °C, the temperature of the mesophase to crystal transition of HMS-5. Samples were also cooled at 20 °C/min from 190 to 157 °C, the transition temperature of the isotropic phase to mesophase transition, held for 40 min, and then cooled at 20 °C/min to 127 °C for further isothermal crystallization.

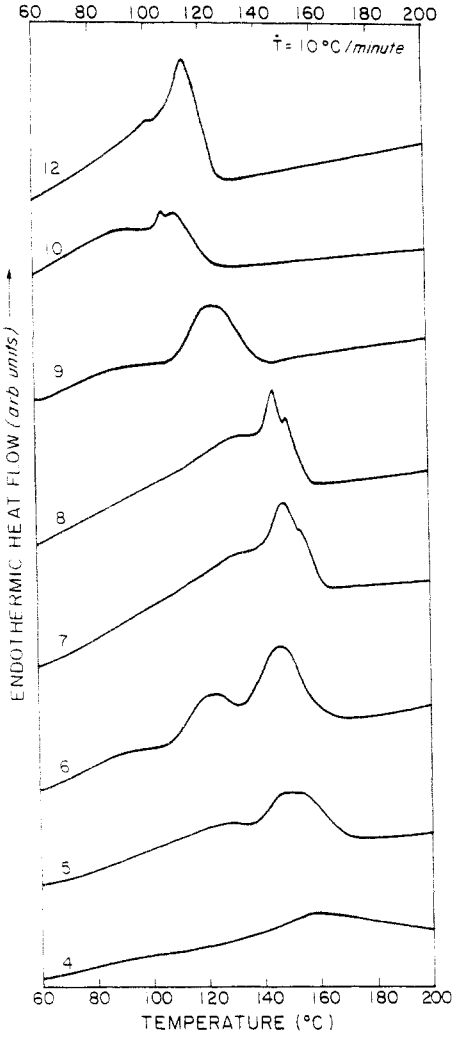

Figure 2. DSC thermograms of HMS-4-10 and -12 at 10 °C/min heating rate.

2.4. Wide-Angle X-ray Scattering. Wide-angle X-ray scattering (WAXS) was performed at room temperature using a Philips PW1830 X-ray generator operated at 45 kV and 45 mA with Ni-filtered Cu Kα radiation (λ = 1.54 Å). The Statton camera used in this study consists of a pinhole collimator over which the sample is placed and a flat film (Kodak DEF-5) to record the scattering pattern. The sample to film distance is calibrated using a Si powder reference standard (from the National Institute of Standards and Technology) rubbed on the sample surface. The first 2θ value for Si is 28.4°. HMS-5 fiber was hand drawn from the mesophase using tweezers. This fiber cooled rapidly in air and will be referred to as raw fiber. Raw fiber was subsequently annealed below the melting temperature at 135 °C for 1 h. WAXS was performed on both the raw and annealed fibers.

3. Results

3.1. Differential Scanning Calorimetry. DSC thermograms of HMS-4-10 and -12 are shown in Figures 1 and 2 for first cooling and second heating, respectively. Nearly all samples showed a dual exothermic response indicating a small higher temperature exotherm representing the isotropic to mesophase (i–lc) transition, followed by a large exotherm at the mesophase to crystalline (lc–k) transition. On the reheating scans, usually dual endotherms were observed. Notice that the upper melting temperature range is quite broad and always covers the temperature range of the isotropic to mesophase transition seen in the cooling scan. Table 1 summarizes the melting and crystallization peak positions. Transition temperature vs n is shown in Figure 3 (cooling) and Figure 4 (heating).

Table 1. Thermal Transition Peak Temperatures for HMS Series Polycarbonates at 10 °C/min Scan Rate

	crystallization temp (°C)		melting temp (°C)	
sample n	T_c(upper) (±2 °C)	T_c(lower) (±1 °C)	T_m(upper) (±1 °C)	T_m(lower) (±1 °C)
4	*a*	129	159	*a*
5	156	132	148	127
6	154	128	147	123
7	144	135	150	131
8	*a*	138	146	136
9	131	106	125	90
10	131	99	109	97
12	*a*	104	116	*a*

[a] No transition seen in this sample.

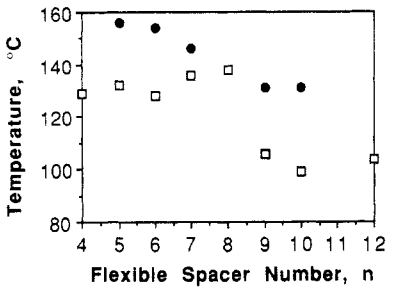

Figure 3. Transition temperatures vs n during cooling: (●) $T_{i\text{-}lc}$ and (□) $T_{lc\text{-}k}$.

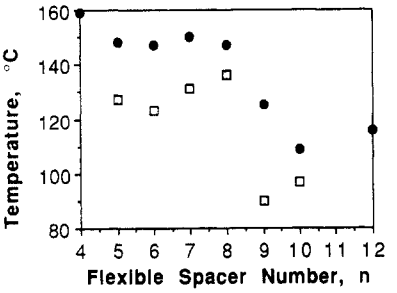

Figure 4. Transition temperatures vs n during heating: (●) upper melting T_{m2} and (□) lower melting T_{m1} peak position.

Table 2. Estimated $\Delta H_{i\text{-}lc}$ and $\Delta H_{lc\text{-}k}$ for HMS Series Polycarbonates at 10 °C/min Scan Rate

sample n	$\Delta H_{i\text{-}lc}$ (kJ/mol)	$\Delta H_{lc\text{-}k}$ (kJ/mol)
4	*a*	0.6
5	0.1	4.3
6	0.2	2.5
7	0.2	4.4
8	*a*	3.6
9	0.6	5.6
10	0.3	4.5
12	*a*	7.8

[a] No transition seen in this sample.

There is only a weak odd–even effect seen at the upper crystalline melting temperature in heating for low n, but no odd–even effect is seen in cooling. The stability range of the mesophase becomes smaller from n = 5 to 8 in the cooling scan. For $n \geq 9$, all the transition temperatures drop. Table 2 lists the estimated $\Delta H_{i\text{-}lc}$ and $\Delta H_{lc\text{-}k}$.

Figure 5 shows DSC scans at cooling rates of 5, 10, 20, and 50 °C/min for HMS-9. There is little change for the isotropic to mesophase transition temperature (indicated by an arrow) with the cooling rate, but the onset of crystallization is suppressed by higher cooling rate. Similar results were seen in HMS-6. The liquid crystalline phase transition is not affected much by this variation of cooling rate for these two samples. However, the formation of three-dimensional crystals is greatly affected by the cooling

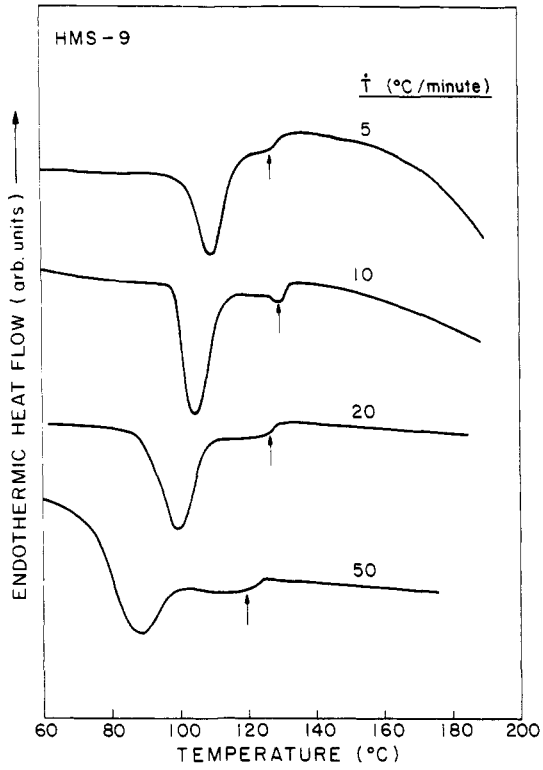

Figure 5. DSC thermograms of HMS-9 at 5, 10, 20, and 50 °C/min cooling rates.

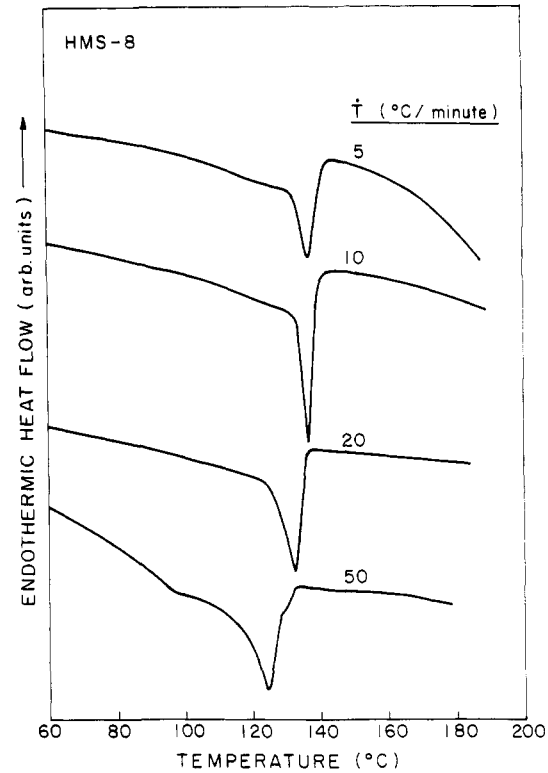

Figure 6. DSC thermograms of HMS-8 at 5, 10, 20, and 50 °C/min cooling rates.

rate due to the strong temperature dependence of the rate of formation of secondary nuclei.

In Figure 1, we were unable to observe the isotropic to mesophase transition for HMS-8, which we had expected to see at the front shoulder of the large crystallization exotherm, as was the case for HMS-5–7. Given the dependency of the crystallization exotherm on cooling rate, we used a high cooling rate to suppress the exotherm of crystallization, causing it to occur at a lower temperature. Figure 6 shows DSC scans of HMS-8 at cooling rates of 5, 10, 20, and 50 °C/min. At a cooling rate of 50 °C/min HMS-8 now clearly shows the mesophase transition as a shoulder on the high-temperature side of the crystallization exotherm. It is not seen at lower cooling rates because it overlaps with the crystallization phase transition and cannot be separately identified. A similar effect of cooling rate was seen for HMS-7. The mesophase transition of HMS-7 can be observed at cooling rates of 5–50 °C/min (see Figure 1 for 10 °C/min) but disappears at a slow cooling rate of 2 °C/min. At this rate, the onset temperature of the transition from the isotropic to crystalline phase is about 143 °C. Table 3 summarizes the onset temperatures of the transitions from the isotropic to mesophase (T_{i-lc}) and from the mesophase to crystalline phase (T_{lc-k}). All the heats of transition from the isotropic to mesophase are qualitatively the same with the cooling rates.

During isothermal crystallization, the crystallization time, t_c, is the time after which no further exothermic heat flow can be detected. As the crystallization temperature increases, the crystallization time increases, and the exothermic peak area decreases and finally becomes undetectable. Figure 7 shows the isothermal crystallization heat flow versus time for HMS-9 crystallized at 108 and 120 °C. As the crystallization temperature increases, the crystallization kinetics become slower, and the area under the exothermic peak also becomes smaller. Tables 4 and 5 summarize the time to maximum exothermic heat flow and crystallization time as a function of the crystallization temperature from the isothermal study of HMS-5–8. Table 6 summarizes both the time to maximum exothermic heat flow and crystallization time as a function of the crystallization temperature for HMS-9.

Figure 8 shows DSC scans of HMS-9 at a heating rate of 5 °C/min after staying at the crystallization temperature isothermally until crystallization was finished. The sample is not cooled before scanning; therefore this technique is called an "immediate rescan". These thermograms represent the immediate rescans after isothermal crystallization at 108, 112, 114, 116, 118, 120, and 123 °C. We can see that there are two major peaks in nearly all the immediate rescan endotherms. We will designate the lower one as T_{m1} and the upper one as T_{m2}, according to the peak position. T_{m2} is broader and extends to the bottom of T_{m1}. The area under T_{m2} becomes smaller as the crystallization temperature increases. Finally, when crystallization temperature equals 123 °C, only the lower peak remains. Also, the temperature range of T_{m2} becomes smaller and appears to have a fixed upper limit. We observed similar results for the DSC scans of HMS-5, -6, and -8. In each case, there are two endotherms, the upper one of which becomes relatively smaller as crystallization temperature increases.

Figure 9 shows the immediate rescans at heating rates of 1, 2, and 5 °C/min for HMS-9 which was isothermally crystallized at a crystallization temperature of 114 °C. There is little change in T_m and also the area under the melting peak is almost the same with these heating rates. Similar results were also seen for HMS-5. Therefore, we suggest that there is little or no reorganization during this process. This is consistent with studies on other kinds of main chain thermotropic LCPs.[22,23]

Figure 10 shows DSC scans at heating rate of 5 °C/min for HMS-9 after being held at T_c = 114 °C for 0.5, 1.0, 2.0, or 4.7 min. For HMS-9 at this crystallization temperature, the time to maximum exothermic heat flow is 0.6 min as determined from isothermal crystallization studies. From this study of HMS-9, we see that there are two peaks developing at the same time. By comparing the melting

Table 3. Onset Temperatures of Transitions of HMS-6–9 at Different Cooling Rates

	HMS-6		HMS-7		HMS-8		HMS-9	
cooling rate (°C/min)	T_{i-lc} (°C) (±1 °C)	T_{lc-k} (°C) (±1 °C)	T_{i-lc} (°C) (±1 °C)	T_{lc-k} (°C) (±1 °C)	T_{i-lc} (°C) (±1 °C)	T_{lc-k} (°C) (±1 °C)	T_{i-lc} (°C) (±1 °C)	T_{lc-k} (°C) (±1 °C)
5	156	137	144	141	*a*	143	133	120
10	156	137	143	138	*a*	142	134	114
20	153	123	139	132	*a*	136	133	112
50	150	111	132	121	132	128	126	99

[a] No transition seen at this rate.

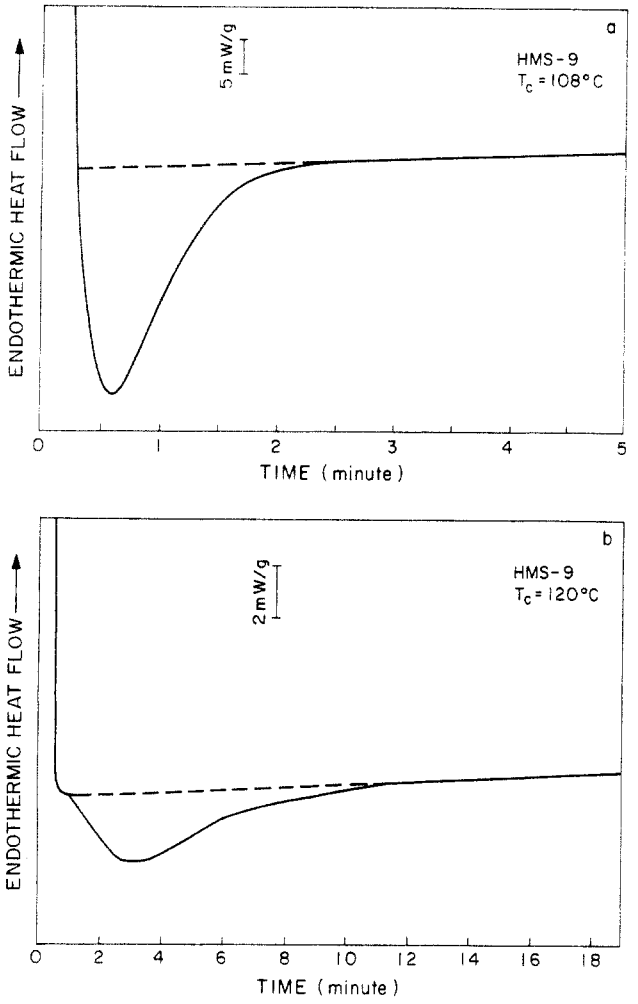

Figure 7. DSC heat flow vs time during isothermal crystallization of HMS-9 at (a) 108 and (b) 120 °C.

Table 4. Time to Maximum Exothermic Heat Flow (min) as a Function of Crystallization Temperature for HMS-5–8

	crystallization temp (°C)						
sample	130	134	138	140	142	144	147
HMS-5	*a*	0.7	0.7	0.9	1.2	1.4	2.2
HMS-6	0.4	0.8	1.3	1.6	1.9	2.1	*a*
HMS-7	*a*	*a*	0.9	1.0	1.4	1.7	3.4
HMS-8	*a*	*a*	0.2	0.4	0.7	1.2	2.6

[a] Not tested at this temperature.

peaks after different crystallization time, we see that the upper peak, T_{m2}, with wider and higher range, stops growing earlier than the lower one, T_{m1}. The upper peak develops most of its area before the time to maximum exothermic heat flow, while the lower peak develops significant area after this time.

3.2. Optical Microscopy. Optical microscopy revealed a fine-grained pattern of birefringence whose intensity (recorded with a photodetector) changed rapidly near the isotropic to mesophase transition and more gradually near

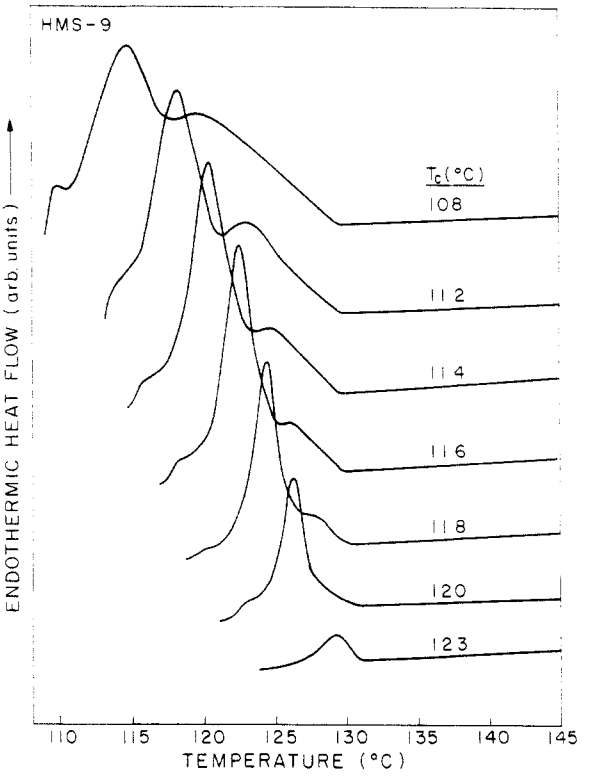

Figure 8. Immediate rescan DSC thermograms of HMS-9 at 5 °C/min heating rate after isothermal crystallization at the temperatures shown.

Table 5. Crystallization Time (min) as a Function of Crystallization Temperature for HMS-5–8

	crystallization temp (°C)						
sample	130	134	138	140	142	144	147
HMS-5	*a*	2.1	2.8	3.0	4.0	8.6	13.7
HMS-6	2.8	4.8	6.3	7.7	8.6	9.3	*a*
HMS-7	*a*	*a*	4.4	5.0	6.3	8.0	12.4
HMS-8	*a*	*a*	2.0	2.8	4.1	8.2	17.8

[a] Not tested at this temperature.

Table 6. Time to Maximum Exothermic Heat Flow and Crystallization Time (min) as a Function of Crystallization Temperature for HMS-9

cryst temp (°C)	time to max exothermic heat flow (min)	cryst time (min)
108	0.3	2.2
112	0.5	2.5
114	0.6	4.7
116	1.0	6.7
118	1.4	7.5
120	2.1	10.8
123	2.2	14.2

the mesophase to crystalline transition. Poorly formed spherulites were seen in HMS-5, -6, -7, and -8. None were seen in HMS-4, -9, -10, and -12.

In Figure 11, we show optical micrographs of HMS-5 at a magnification of 320× between crossed polars. We can

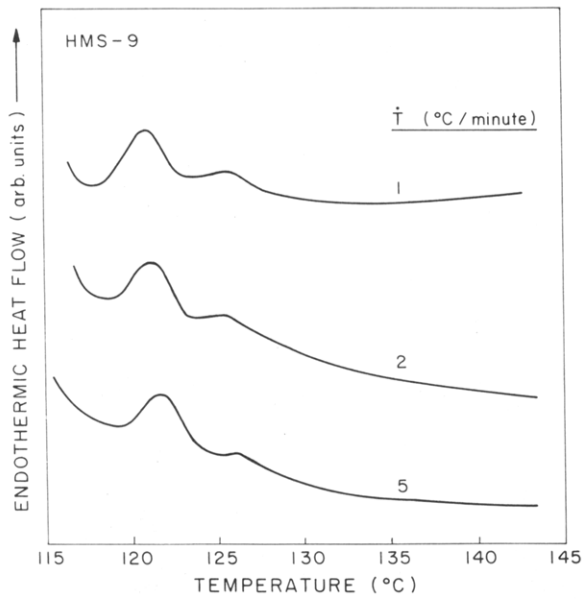

Figure 9. DSC thermograms of HMS-9 after isothermal crystallization at 114 °C for 4.68 min. Immediate rescan at the indicated rates.

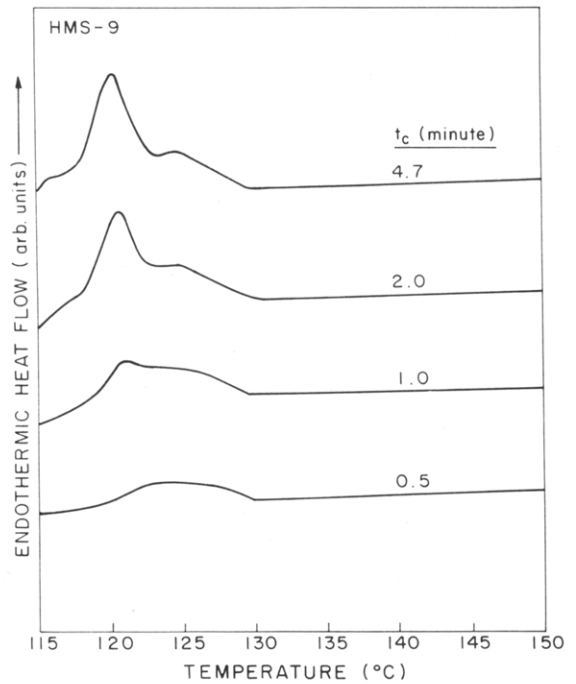

Figure 10. Immediate rescan of HMS-9 at 5 °C/min heating rate after isothermal crystallization at 114 °C for the indicated times.

see a schlieren texture in Figure 11a, which is a characteristic of the nematic mesophase.[24] As shown in Figure 11, spherulites developing at a crystallization temperature of 127 °C without annealing were much bigger than those developing at 127 °C after prior annealing at 157 °C, which is the isotropic to mesophase transition temperature. When the sample was annealed at 157 °C, many small highly birefringent spots formed at this temperature. Upon cooling to 127 °C, the birefringence increased and crystals filled the entire field of view, as shown in Figure 11. We conclude that the locally forming mesophase serves as nucleation site for subsequent crystallization.

3.3. Wide-Angle X-ray Scattering Fiber Pattern. As shown in Figure 12a, the X-ray diffraction pattern of HMS-5 raw fiber shows one diffuse equatorial maximum and no meridional reflections, which is evidence of a

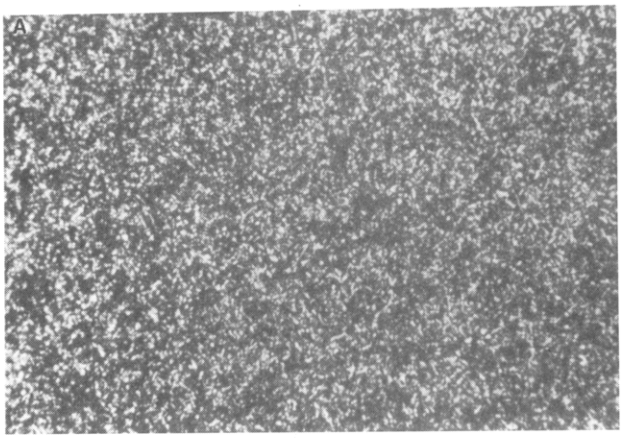

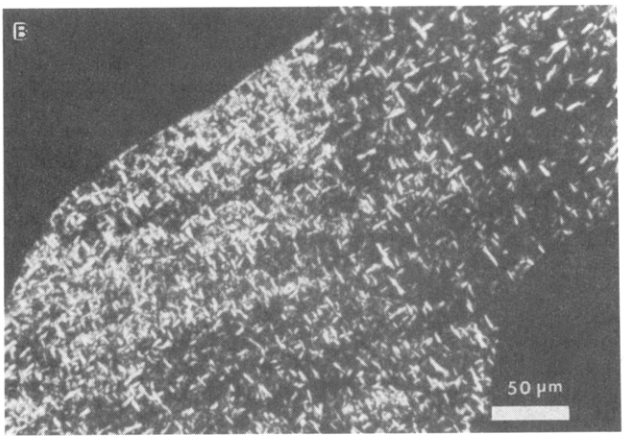

Figure 11. Optical micrograph of HMS-5 crystallized at 127 °C for 40 min: (a) sample annealed at 157 °C for 40 min prior to crystallization at 127 °C; (b) sample cooled directly to 127 °C without annealing. Scale marker is the same for both figures.

nematic mesophase.[15] After the raw fiber is annealed below the melting point, an oriented fiber diffraction pattern is seen, as in Figure 12b. One meridional reflection was observed in the fiber diffraction pattern of the annealed fibers. In Figure 12b, two strong equatorial reflections can be seen. The *d* spacings of these peaks are 4.10 and 4.55 Å. The position of the diffuse equatorial maxima seen in the raw fiber diffraction pattern lies in between the positions of the two peaks with maximum intensity seen in the oriented annealed fiber diffraction pattern.

4. Discussion

4.1. Relationship between Transition Temperatures and Flexible Spacer Number. In our HMS polycarbonate polymers, no odd–even effect is seen in any of the transition temperatures, as shown in Figures 3 and 4. In contrast, all of the HMS polyethers[19] and polyesters[14,20] showed an odd–even effect in both the melting temperature and the transition temperature from the liquid crystalline phase to the isotropic phase. We suggest that the conformation of the carbonate linkage causes the loss of the odd–even effect. As mentioned in the Introduction, for most LCPs with rigid rod mesogens, polymers with an even number of methylene units in the flexible spacer have a higher degree of alignment than those with an odd number. Moreover, as with Percec's polyethers,[6–10] when a polymer has a flexible mesogen, the liquid crystal mesophase is formed by the coupled action of the flexible

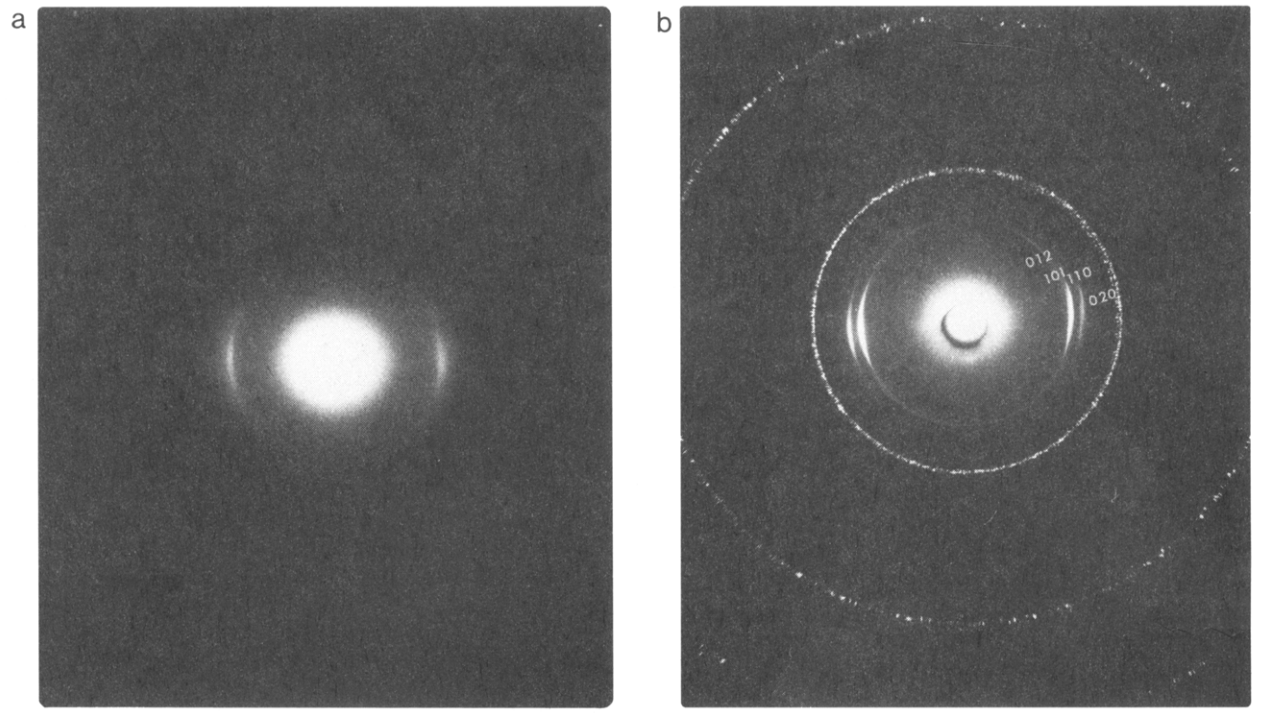

Figure 12. Flat-film wide-angle X-ray scattering pattern of HMS-5 fiber, with fiber axis vertical: (a) raw fiber showing diffuse equatorial maximum; (b) fiber after annealing at 135 °C for 1 h showing crystal lattice reflections.[29] Spotty rings are from silicon powder calibration standard.

mesogen and the flexible spacer. The flexible mesogen can result in significant conformational changes of the polymer chain, which will affect the formation of the liquid crystal mesophase. Similarly, for the HMS polycarbonates reported here, the carbonate linkages positioned beside the methylstilbene mesogen can cause considerable conformational change. In order to form the mesophase, the carbonate linkages have to adopt the conformation that causes the polymer chain to be aligned and stabilized. The specific conformation in the carbonate linkage might be the reason why the odd–even effect is lost within the HMS polycarbonate polymers. The loss of the odd–even effect in the transition temperatures has also been seen in enantiotropic liquid crystalline polycarbonates.[20]

Next, we consider the cause of the melting point reduction in HMS polycarbonates compared to HMS polyethers or polyesters. At the equilibrium melting temperature T_m, the crystal phase is in equilibrium with the melt. Setting the Gibbs free energy change equal to zero, we write

$$T_m = \Delta H_f / \Delta S_f \quad (1)$$

where ΔH_f and ΔS_f are the differences in enthalpy and entropy, respectively, between the melt and the crystal phase. Better intermolecular interaction leads to the higher absolute value of ΔH_f which would tend to increase the melting point. ΔS_f reflects the greater randomness in the isotropic phase.[15] The carbonate linkage contributes more conformational entropy change between the crystalline phase and the isotropic phase and between the isotropic phase and the mesophase than either ester or ether linkages. This effect not only causes the lower melting transition temperature of HMS polycarbonates but also might cause the stable range of their mesophases to become narrowed. Actually, HMS polycarbonates are monotropic liquid crystalline polymers. The local intermolecular interaction is the driving force for crystallization which leads to monotropic behavior. The effect of intermolecular interaction on mesophase behavior has been studied by other groups.[25]

A change in properties occurs when the flexible space number exceeds 8. First, from polarizing optical microscopy, small but ill-formed spherulites are seen for n = 5, 6, 7, and 8. No spherulites large enough to be identified by optical microscopy were seen for n = 9, 10, or 12. Second, in both cooling and heating, the transition temperatures of HMS polycarbonate LCPs drop sharply when n is greater than 8. In HMS polyethers,[19] which have an enantiotropic mesophase, the transition temperatures also drop when $n > 8$. Lowering of the crystallization and melting temperatures and inability to form large spherulites imply that crystal size and perfection are reduced when n exceeds 8.

In terms of the repeat unit structure of the HMS polycarbonates, we note that the change in properties occurs when the length of the flexible spacer group exceeds the length of the stilbene mesogen for chains in the all-trans conformation. From the standpoint of energy minimization, this conformation represents one of the most probable conformations resulting in extended polymer chains for most liquid crystalline polymers in the mesophase.[10,17,26] The fact that the same effect is seen in HMS polycarbonates and in HMS polyethers is related to the similarity of their chemical structures. Both of these LCPs have linking groups that are symmetric. Crystal perfection is related to interchain packing, and in both HMS polycarbonates and polyethers the interchain packing is affected by the relative lengths of the flexible spacer and mesogen. For HMS polyethers, when the mesogen length is greater than that of the flexible spacer, the most stable crystal structure is "intermeshed", in which the interchain packing is tight.[27] However, this kind of crystal structure does not exist in those polymers with a flexible spacer longer than its mesogen, which have a layered structure. Similarly, HMS polycarbonates with a flexible spacer longer than the mesogen do not seem to have an intermeshed structure. In support of this view, we note

that in the plot of d spacing for two major interchain reflections versus flexible spacer number, n, the interchain spacing shows an odd–even effect for low n value but levels off when $n \geq 9$.[28] These results will be more completely discussed in a subsequent publication[29] on the X-ray diffraction of HMS polycarbonates.

When the length of the flexible spacer gets close to that of the mesogen from $n = 5$ to 8, the stability range of the liquid crystalline phase seen in the cooling scan becomes smaller. For HMS-7 and -8, the closeness of the length between the mesogen and the spacer increases the crystallization rate and makes the mesophase transition and the crystallization transition indistinguishable for the lower cooling rates. For these two samples, the liquid crystalline phase is much more unstable than in other samples, as suggested by the results of cooling rate studies in Table 3. We suggest that the difference is related to the difference of the spacer length, which results in the difference in the crystal structure. When the length of the spacer becomes close to that of the mesogen, intermolecular interaction is affected, causing fast crystallization. In another report, we will describe our experiments on the X-ray diffraction of HMS polycarbonate LCPs in which we investigate the change of crystal structure with the number of methylene units in the flexible spacer.[29]

4.2. Crystal Formation. For nematic liquid crystalline polymers, the crystallization from the nematic phase has been widely studied.[22,23,30–33] The nematic phase usually serves as a nucleus for subsequent crystallization. Without the formation of the nematic phase, the polymer crystallizes much more slowly from the isotropic phase. The crystals forming from the nematic phase usually have a structure similar to their nematic phase. For monotropic liquid crystalline polymers, the crystallization from the liquid crystalline phase is rapid. Therefore, their liquid crystalline phase is considered to be more ordered than that of enantiotropic nematic LCPs.[3]

Our HMS polycarbonate polymers are monotropic liquid crystalline polymers. As shown in Figures 1 and 2, the range of the transition from the isotropic phase to the nematic phase seen in the cooling scan overlaps the range of the upper melting peak of the crystals seen in the heating scan. The transition from the isotropic phase to the liquid crystal phase is very close in temperature to the transition from the liquid crystal phase to the crystal phase for the heating and cooling rates used in this study.

For main chain thermotropic liquid crystalline polymers, dual endotherms are usually seen in the DSC heating scan. As shown in Wendorff's crystallization studies on liquid crystalline copolyesters,[30] two groups of crystals develop in sequence. The upper melting crystals form first from the nematic phase and restrict the growth of the later crystals forming among the first crystals by an annealing process. The closeness of the peak temperatures of the dual endotherms is a characteristic of our HMS polycarbonate LCPs. Whether we heat by immediately rescanning after isothermal crystallization or heat after cooling from the melt, two crystal populations are observed. Each crystal population melts predominantly to form one of the dual endotherms. We conclude that the first crystal group using the nematic phase as the nuclei for crystallization has a faster crystallization rate. The second crystal group grows more slowly due to the slower rate of formation of secondary nuclei from the isotropic phase.

The upper peak seen in the immediate rescan after isothermal crystallization is from the melting of the crystals developing from the nematic phase, while the lower peak is from the crystals growing from the isotropic phase. These two groups of crystals are both stable, which is why we observe no "reorganization" during the rescan process. The upper melting crystals develop earlier than the lower melting crystals, as shown in Figure 10. Both crystal populations grow fast provided the crystallization temperature is below the transition temperature from the isotropic phase to the nematic phase. As the crystallization temperature increases, the population of upper melting crystals, using the nematic phase as the nuclei for crystallization, gradually diminishes, as shown in Figure 8. This result is in agreement with the observation of decreased exothermic area shown in Figure 7. The mesophase transition covers a broad temperature range of about 10 °C (see Figure 1). The amount of seed nuclei from the mesophase decreases as the isothermal crystallization temperature increases through the mesophase transition range, and this causes reduced ultimate crystallinity. However, the crystallization rate of the lower melting crystal group also slows down. Therefore, the formation of secondary nuclei is also related to the ability of the polymer to form aligned structures.

From the above discussion, we can conclude that the crystals using the nematic phase as the nuclei for crystallization are the crystals which cause the major exotherm right after the transition from the isotropic phase to the nematic phase seen in the cooling scan, as shown in Figure 1. These crystals are also the crystals which cause the upper melting peak in the heating scan, as shown in Figure 2. The lower endotherm, which overlaps greatly with the upper endotherm, is from the melting of those crystals developing from the secondary nuclei forming from the isotropic phase. The closeness of the melting point of these two groups of crystals can be understood by considering the structure of HMS polycarbonate. Due to the flexibility caused by the carbonate linkage, the first group of crystals develops from the nematic phase in regions quite scattered throughout the melt. These crystals have widely varying degrees of perfection, which causes a broad upper endotherm. And these crystals restrict the growth of the later crystals, but not as much as Wendorff's copolyesters do.[30] In the copolyesters LCPs, clearly separate dual endotherms are observed.

The upper melting crystals are very stable and the crystals developing later from the remaining isotropic phase can only develop in a restricted geometry among the first crystals. There is further evidence provided by the crystallization study using optical microscopy. Bigger spherulites were seen within those samples crystallizing without annealing at the isotropic to nematic transition temperature. The annealing caused scattered nematic phases to form locally, which later crystallize and restrict the development of large spherulites. The mechanism of crystallization whereby the secondary crystals develop among the first crystals was actually seen in a transmission electron microscopy study of PEEK.[34] The dual endotherm was also seen in the heating scan of PEEK which had been crystallized from the melt.[35–37] This mechanism of crystallization is common in those polymers with a low degree of crystallinity and generally results in observation of broad endotherms.

5. Conclusions

1. HMS polycarbonates are monotropic liquid crystalline polymers, while HMS polyesters and polyethers have an enantiotropic liquid crystal phase.

2. The conformation in the carbonate linkage strongly affects the stability of the liquid crystal phase and causes the loss of the odd–even effect. The spacer length also

affects the crystallization kinetics. The crystallization from the nematic phase becomes faster when the length of the spacer gets close to that of the mesogen. When the former exceeds the latter, all the transition temperatures drop.

3. The melting of crystals forming directly from the nematic phase causes the high-temperature endotherm seen in the heating scan. These crystals grow fast and restrict the development of the later crystals forming from the isotropic phase. The later crystals are less perfect and melt to form the lower temperature endotherm.

Acknowledgment. This work was supported by the Natick Research, Development and Engineering Center (H.S.-G.) under the auspices of the U.S. Army Research Office Scientific Services Program administered by Battelle (Delivery Order 267, Contract No. DAAL03-91-0034).

References and Notes

(1) Bluhm, A. L.; Cebe, P.; Schreuder-Gibson, H. L.; Stapler, J. T.; Yeomans, W. *Mol. Cryst. Liq. Cryst.* **1994**, *239*, 123.
(2) Percec, V.; Keller, A. *Macromolecules* **1990**, *23*, 4347.
(3) Pardey, R.; Zhang, A.; Gabori, P. A.; Harris, F. W.; Cheng, S. Z. D.; Adduci, J.; Facinelli, J. V.; Lenz, R. W. *Macromolecules* **1992**, *25*, 5060.
(4) Papadimitrakopoulos, F.; Hsu, S. L.; MacKnight, W. J. *Macromolecules* **1992**, *25*, 4761.
(5) Papadimitrakopoulos, F.; Sawa, E.; MacKnight, W. J. *Macromolecules* **1992**, *25*, 4682.
(6) Percec, V.; Tsuda, Y. *Macromolecules* **1990**, *23*, 3509.
(7) Percec, V.; Yourd, R. *Macromolecules* **1989**, *22*, 524.
(8) Percec, V.; Yourd, R. *Macromolecules* **1989**, *22*, 3229.
(9) Cheng, S. Z. D.; Yandrasits, M. A.; Percec, V. *Polymer* **1991**, *32*, 1284.
(10) Yandrasits, M.; Cheng, S. Z. D.; Zhang, A.; Cheng, J.; Wunderlich, B.; Percec, V. *Macromolecules* **1992**, *25*, 2112.
(11) Fujishiro, K.; Lenz, R. W. *Macromolecules* **1992**, *25*, 81.
(12) Blumstein, R. B.; Blumstein, A. *Mol. Cryst. Liq. Cryst.* **1988**, *165*, 361.
(13) Blumstein, A.; Thomas, O. *Macromolecules* **1982**, *15*, 1264.
(14) Blumstein, A. *Polym. J.* **1985**, *17* (1), 277.
(15) Donald, A. M.; Windle, A. H. *Liquid Crystalline Polymers*; Cambridge University Press: Cambridge, 1992.
(16) Abe, A. *Macromolecules* **1984**, *17*, 2280.
(17) Yoon, D. Y.; Bruckner, S. *Macromolecules* **1985**, *18*, 651.
(18) Dobbs, E. C.; Goldberg, L.; Lawson, W.; Robinson, R. *Proc. R. Soc. London* **1939**, *B127*, 140.
(19) Percec, V.; Shaffer, T. D.; Nava, H. *J. Polym. Sci., Polym. Lett.* **1984**, *22*, 637.
(20) Ruviello, A.; Sirigu, A. *Makromol. Chem.* **1982**, *183*, 895.
(21) Sato, M.; Nakatsuchi, K.; Ohkatsu, Y. *Makromol. Chem., Rapid Commun.* **1986**, *7*, 231.
(22) Carpaneto, L.; Marsano, E.; Valenti, B.; Zanardi, G. *Polymer* **1992**, *33*, 3865.
(23) Warner, S. B.; Jaffe, M. *J. Cryst. Growth* **1980**, *48*, 184.
(24) Noel, C. In *Liquid Crystal Polymers: From Structure to Applications*; Collyer, A. A., Ed.; Elsevier Science Publishers Ltd.: London, 1992.
(25) Papadimitrakopoulos, F.; Kantor, S. W.; MacKnight, W. J. In *Fiber and Polymer Science, Recent Advances*; Fornes, R. E., Gilbert, R. D., Eds.; VCH Publishers: New York, 1992.
(26) Aharoni, S. M.; Correale, S. T.; Hammond, W. B.; Hatfield, G. R.; Murthy, N. S. *Macromolecules* **1989**, *22*, 1137.
(27) Unger, G.; Keller, A. *Mol. Cryst. Liq. Cryst.* **1988**, *155*, 313.
(28) Cebe, P.; Carbeck, P.; Schreuder-Gibson, H. *Polym. Prepr. (Am. Chem. Soc., Div. Polym. Chem.)* **1992**, *33* (1), 331.
(29) Cheng, Y.-Y.; Cebe, P.; Schreuder-Gibson, H.; Bluhm, A. L.; Yeomans, W.; Capel, M. *Mol. Cryst. Liq. Cryst.*, to be submitted.
(30) Butzbach, G. D.; Wendorff, J. H.; Zimmermann, H. J. *Polymer* **1986**, *27*, 1337.
(31) Bisvas, A.; Blackwell, J. *Macromolecules* **1988**, *21*, 3146.
(32) Bisvas, A.; Blackwell, J. *Macromolecules* **1988**, *21*, 3152.
(33) Bisvas, A.; Blackwell, J. *Macromolecules* **1988**, *21*, 3158.
(34) Bassett, D. C.; Olley, R. H.; Al Raheil, I. A. M. *Polymer* **1988**, *29*, 1745.
(35) Blundell, D. J.; Osborn, B. N. *Polymer* **1983**, *24*, 953.
(36) Cebe, P.; Hong, S.-D. *Polymer* **1986**, *27*, 1183.
(37) Cheng, S.; Cao, M.-Y.; Wunderlich, B. *Macromolecules* **1986**, *19*, 1868.